
Article:
Degen, G.E. orcid.org/0000-0002-0804-4169, Jackson, P.J. orcid.org/0000-0001-9671-2472, Proctor, M.S. orcid.org/0000-0002-1484-850X et al. (3 more authors) (2023) High cyclic electron transfer via the PGR5 pathway in the absence of photosynthetic control. Plant Physiology, 192 (1). pp. 370-386. ISSN 0032-0889

https://doi.org/10.1093/plphys/kiad084

Short title: Cyclic electron transfer and PSI photoprotection

High cyclic electron transfer via the PGR5 pathway in the absence of photosynthetic control

Gustaf E. Degen[1], Philip J. Jackson[1,2], Matthew S. Proctor[1], Nicholas Zoulias[1], Stuart A. Casson[1] and Matthew P. Johnson[1*]

[1]Plants, Photosynthesis and Soil, School of Biosciences, University of Sheffield, Firth Court, Western Bank, Sheffield, S10 2TN, UK.

[2]Department of Chemical and Biological Engineering, University of Sheffield, Sheffield, S1 4NL, UK.

Corresponding Author Email: matt.johnson@sheffield.ac.uk

The author responsible for distribution of materials integral to the findings presented in this article in accordance with the policy described in the Instructions for Authors (https://academic.oup.com/plphys/pages/General-Instructions) is Matthew P. Johnson.

One-sentence summary: High PGR5-depedent cyclic electron transfer increases proton motive force but in the absence of ATP synthase regulation is insufficient to induce photosynthetic control.

Author contributions: G.E.D, M.S.P, P.J.J and N.Z performed research, S.A.C and M.P.J supervised research, G.E.D analyzed the data and G.E.D and M.P.J wrote the paper. All authors approved of the manuscript prior to submission.

Abstract

The light reactions of photosynthesis couple electron and proton transfers across the thylakoid membrane, generating NADPH, and proton motive force (pmf) that powers the endergonic synthesis of ATP by ATP synthase. ATP and NADPH are required for CO_2 fixation into carbohydrates by the Calvin-Benson-Bassham cycle (CBBC). The dominant ΔpH component of the pmf also plays a photoprotective role in regulating photosystem II (PSII) light harvesting efficiency through non-photochemical quenching (NPQ) and photosynthetic control via electron transfer from cytochrome b_6f (cytb_6f) to photosystem I (PSI). ΔpH can be adjusted by increasing the proton influx into the thylakoid lumen via upregulation of cyclic electron transfer (CET) or decreasing proton efflux via downregulation of ATP synthase conductivity (gH^+). The interplay and relative contributions of these two elements of

ΔpH control to photoprotection are not well understood. Here, we showed that an Arabidopsis (*Arabidopsis thaliana*) ATP synthase mutant *hunger for oxygen in photosynthetic transfer reaction 2* (*hope2*) with 40% higher proton efflux has supercharged CET. Double crosses of *hope2* with the CET-deficient *proton gradient regulation 5* and *ndh-like photosynthetic complex I (ndho)* lines revealed that PGR5-dependent CET is the major pathway contributing to higher proton influx. PGR5-dependent CET allowed *hope2* to maintain wild-type levels of ΔpH, CO_2 fixation and NPQ, however photosynthetic control remained absent and PSI was prone to photoinhibition. Therefore, high CET in the absence of ATP synthase regulation is insufficient for PSI photoprotection.

Keywords

Photoprotection, cyclic electron transfer, ATP synthase, non-photochemical quenching, photosynthetic control, photosystem I.

Introduction

CO_2 fixation into biomass during photosynthesis requires reducing power in the form of NADPH and energy in the form of ATP (Kramer and Evans, 2010). NADPH is provided by coupled photosynthetic linear electron transfer (LET) reactions in the thylakoid membrane, which also generate pmf for ATP synthesis via ATP synthase. In chloroplasts, pmf is largely composed of the proton concentration gradient (ΔpH), with minimal contribution from the membrane potential (ΔΨ) in the steady state (Wilson et al., 2021), which is detrimental to productive charge separation in PSII (Davis et al., 2016) and largely dissipated by counterion movements (Hind et al., 1974). In addition to its manifest role in ATP synthesis, the ΔpH also plays a vital role in regulating photosynthetic electron transfer and light harvesting reactions via photosynthetic control and energy-dependent NPQ, known as qE (Li et al., 2009; Malone et al., 2021). Photosynthetic control restricts the rate of plastoquinol (PQH_2) oxidation at cytb_6f activity, can be measured as the donor-side limitation of PSI (Y(ND)) using P700 absorption spectroscopy and protects PSI against photo-oxidative damage in excess light (Jahns et al., 2002; Suorsa et al., 2013). By contrast, qE involves ΔpH induced protonation of the PsbS protein and de-epoxidation of the light harvesting antenna complex II (LHCII)-bound xanthophyll violaxanthin to zeaxanthin, which collectively bring about energy dissipation in LHCII, protecting PSII from photo-oxidative damage (Ruban et al., 2012). qE can be measured as the rapidly-relaxing component of NPQ using pulse-amplitude modulated chlorophyll fluorescence. These ΔpH-dependent regulatory mechanisms are critical to plant growth in fluctuating light environments and rely on the careful modulation of the proton influx/ efflux reactions across the thylakoid membrane (Armbruster et al., 2017).

66 Proton efflux is regulated primarily by the conductivity (gH^+) and abundance of the chloroplast
67 ATP synthase (Kramer et al., 2004). Antisense mutants of the γ-subunit in *Nicotiana benthamiana*
68 showed that ATP synthase levels could be reduced by 50% without affecting gH^+ or pmf, while further
69 decreases diminished gH^+ and increased pmf leading to higher qE and Y(ND) (Rott et al., 2011).
70 Regulation of the ATP synthase activity is therefore a key element of proton efflux control. Two types
71 of regulation have been described for ATP synthase; redox and metabolic control (Mills and Mitchell,
72 1982; Ort and Oxborough, 1992; Kanazawa and Kramer, 2002; Kohzuma et al., 2013). Redox control
73 of ATP synthase is mediated by the reduction-oxidation status of two regulatory cysteines (C202, C208
74 in *Arabidopsis thaliana*) which form a disulfide bridge stabilizing a loop of the γ1-subunit that acts as
75 a chock, interfering with the rotation of the catalytic F1 head of the enzyme involved in ATP synthesis
76 (Hisabori et al., 2003; Hahn et al., 2018). Therefore a lower threshold pmf is required to activate the
77 reduced enzyme (Junesch and Gräber, 1987). Upon illumination, activation of LET causes reduction of
78 Fd and NADPH, these can reduce thioredoxin (TRX) proteins via the Fd dependent thioredoxin
79 reductase (FTR) or NADPH dependent thioredoxin reductase (NTRC) enzymes. TRX then reduces the
80 regulatory disulfide in the γ1-subunit (Carrillo et al., 2016; Sekiguchi et al., 2020). By contrast,
81 inactivation of LET in the dark leads to gradual oxidation of the regulatory cysteines by 2-Cys
82 peroxiredoxin (PRX), restoring the higher pmf threshold for activation (Ojeda et al., 2018). In addition
83 to redox control, gH^+ is known to be modified by varying NADPH, CO_2 and Pi concentration suggesting
84 ATP synthase is also under metabolic control (Kanazawa and Kramer, 2002; Avenson et al., 2005;
85 Takizawa et al., 2008; Kohzuma et al., 2013). Though the mechanism of metabolic control of ATP
86 synthase remains to be elucidated. The *mothra* mutant of Arabidopsis has changes in three conserved
87 acidic residues in the γ1-subunit (D211V, E212L and E226L) resulting in the loss of redox sensitivity
88 (Kohzuma et al., 2012). The pmf threshold for activation in *mothra* is correspondingly higher resulting
89 in a lower gH^+, increased pmf, increased qE and lower LET rate, yet gH^+ varies with CO_2
90 concentrations, suggesting that metabolic control is unaffected. By contrast, in the Arabidopsis γ1-
91 subunit mutant *hope2* (hunger for oxygen in photosynthetic electron transport 2, a G134D amino acid
92 change in a putative NADP(H)-binding motif in the Rossman fold), renders gH^+ insensitive to changing
93 CO_2 concentration, although redox control appears normal (Takagi et al., 2017). Interestingly, *hope2*
94 showed a different phenotype to *mothra* with increased gH^+, the virtual absence of Y(ND) and a greater
95 susceptibility to PSI photoinhibition, although maximum LET rate and CO_2 assimilation were
96 unaffected. Crucially, the phenotype of *hope2* was successfully ameliorated via complementation with
97 a WT copy of the γ1-subunit.

98 Proton influx can occur via one of several coupled electron transfer pathways. LET involves
99 the light-powered transfer of electrons from water to $NADP^+$, via a chain including PSII, plastoquinone
100 (PQ)/PQH_2, cytb_6f, plastocyanin (Pc), PSI, ferredoxin (Fd) and ferredoxin-$NADP^+$ reductase (FNR).
101 Unlike LET, alternative electron flows can contribute to pmf generation without generating net

102 NADPH. These include; pseudo-cyclic electron transfer (water-water cycle), where electrons from Fd
103 are instead transferred to oxygen via flavodiiron (Flv) proteins to form water; the Mehler reaction,
104 where PSI directly reduces oxygen to superoxide; and the malate valve, where NADPH is consumed to
105 reduce oxaloacetate to malate, which can be exported from the chloroplast to be oxidized in the
106 mitochondria (Miyake, 2010; Alric and Johnson, 2017). However, in angiosperms such as Arabidopsis,
107 Flv proteins are absent and the primary alternative electron flow is cyclic electron transfer (CET), where
108 electrons from Fd reduce PQ forming a cycle around PSI and cytb_6f via Fd-PQ reductase activity (FQR)
109 (Johnson, 2011; Yamori and Shikanai, 2015). Two CET pathways occur in Arabidopsis, one sensitive
110 to the inhibitor antimycin-A (AA) involves the PROTON GRADIENT REGULATION 5 (PGR5)
111 protein (referred to as CET1) and the second is catalyzed by the NDH-like photosynthetic Complex I
112 (NDH, referred to as CET2) (Yamori and Shikanai, 2015). How PGR5 mediates CET1 remains
113 unknown, early ideas that it acts together with PGR5-LIKE 1 (PGRL1) to form an FQR (DalCorso et
114 al., 2008; Hertle et al., 2013) were recently invalidated by evidence showing that PGRL1 channels
115 PGR5 activity and protects PGR5 from degradation by PGR5-LIKE 2 (PGRL2) (Rühle et al., 2021).
116 An alternative suggestion is that the cytb_6f complex binds FNR and together they play the role of the
117 FQR (Shahak et al., 1981; Joliot and Johnson, 2011). However while cytb_6f can be co-purified with
118 FNR (Clark et al., 1984; Zhang et al., 2001), to date no FNR- cytb_6f -PGR5 complex possessing the
119 requisite FQR activity, which can be as high as 130 e^{-1} s^{-1} in Arabidopsis (Joliot et al., 2004), has been
120 isolated. By contrast, high-resolution structures of the NDH-PSI CET2 supercomplex from Arabidopsis
121 and barley (*Hordeum vulgare*) have been described (Shen et al., 2022; Su et al., 2022). The Arabidopsis
122 *ndho* and *crr* mutants, which both lack NDH-dependent CET2, have relatively mild phenotypes with
123 only slight differences seen in pmf generation and photosynthetic activity (Munekage et al., 2004; Wang
124 et al., 2015; Nikkanen et al., 2018). On the other hand, the Arabidopsis *pgr5* mutant suffers a substantial
125 loss of ΔpH, qE and Y(ND) in high light together with lower LET, CO_2 assimilation and increased PSI
126 photoinhibition (Munekage et al., 2004; Suorsa et al., 2012; Nikkanen et al., 2018). The more severe
127 phenotype of *pgr5* suggests that CET1 is the dominant pathway in Arabidopsis and that NDH-dependent
128 CET2 has a limited capacity to compensate. A number of high cyclic electron flow (*hcef)* mutants have
129 been described in Arabidopsis and *Nicotiana benthamiana* (Livingston et al., 2010a; Livingston et al.,
130 2010b; Strand et al., 2017). Yet to date, those *hcef* mutants characterized in detail have only shown
131 upregulation of the NDH-dependent CET2 pathway (Livingston et al., 2010a; Livingston et al., 2010b;
132 Strand et al., 2017), leading some to speculate that PGR5 may not be directly involved in CET (Suorsa
133 et al., 2012; Takagi and Miyake, 2018). Interestingly, *pgr5* also shows a high gH^+ phenotype, leading
134 to the suggestion that it may alternatively regulate ATP synthase (Avenson et al., 2005). However, to
135 date no interaction between these proteins has been observed. Moreover, overexpression of pseudo-
136 CET inducing Flv proteins from *Physcomitrium* in the *pgr5* mutant was able to restore pmf to WT levels
137 and ameliorated the high gH^+ phenotype, arguing against direct regulation of ATP synthase by PGR5
138 (Yamamoto et al., 2016). The low pmf in *pgr5* is also unlikely to be the cause of the high gH^+ since low

139 pmf in the Arabidopsis *pgr1* mutant of cytb_6f was accompanied by contrastingly low gH^+ (Yamamoto
140 and Shikanai, 2020). Therefore, the cause of high gH^+ in *pgr5* remains unknown.

141 The fact that *hope2* and *pgr5* mutants share a low Y(ND), high gH^+ phenotype but differ in their
142 respective capacities for qE, CO_2 assimilation and LET (Munekage et al., 2004; Takagi et al., 2017)
143 suggests that proton influx and efflux may play distinct roles in photosynthetic regulation. Here, we
144 investigated these relationships further by creating double mutants lacking *hope2* and either *ndho* or
145 *pgr5*. The results unexpectedly demonstrate that loss of ATP synthase regulation in *hope2* is
146 compensated for by increased PGR5-dependent CET, which maintains ΔpH and qE but fails to restore
147 photosynthetic control.

148

149 # Results

150 ## *hope2* maintains wild-type levels of pmf due to increased proton flux

151 We first sought to confirm that the CO_2 assimilation (A) phenotype of *hope2* was WT-like as previously
152 reported (Takagi et al., 2017). Indeed, A in *hope2* was similar to WT Col-0 at both high and low light
153 intensity, although between 100 and 275 µmol photons m^{-2} s^{-1} A was slightly lower in *hope2* (Figure
154 1a). The A/Ci response in *hope2* was not significantly different to the WT Col-0 (Figure 1b). By
155 contrast, in *pgr5* we find A in response to light and varying intercellular CO_2 concentrations (Ci) is
156 lower compared to the WT *gl1* (Figure 1a and b). To estimate maximum Rubisco carboxylation rates
157 *in vivo* ($V_{c,max}$) and maximum electron transport rate used in RuBP regeneration (J_{max}), we fit the
158 Farquhar-von Caemmerer-Berry (FvCB) model (Farquhar et al., 1980) to individual A/Ci curves. $V_{c,max}$
159 and J_{max} were not different in *hope2* compared to Col-0 ($p > 0.05$), confirming that carbon fixation is
160 not limited, in contrast to CET1-deficient *pgr5* ($p < 0.05$). This confirms that despite sharing the high
161 gH^+ phenotype with *pgr5*, *hope2* is still able to maintain an optimal ATP/NADPH ratio for CO_2
162 assimilation.

163 We investigated how *hope2* is able to achieve WT-like CO_2 assimilation further by comparing
164 the generation of pmf in *hope2* and *pgr5* during photosynthetic induction. During the first 50 s of
165 illumination, pmf in *hope2* was lower compared to *pgr5* and WT (Figure 1c), due to increased gH^+
166 levels (Figure 1d), while proton flux (vH^+) was similar to *pgr5* and WT (Figure 1e). Thus, during the
167 first 50 s of photosynthetic induction gH^+ regulation makes a larger contribution to pmf than vH^+. After
168 3 min, pmf in *hope2* reached WT levels, despite high gH^+, due to strongly increased vH^+ (Figure 1c-e).
169 By contrast, pmf in *pgr5* dropped continuously during the first ~200 s of actinic light exposure due to
170 a combination of increasing gH^+ and low vH^+ (Figure 1c-e). Therefore, on longer timescales increases
171 in vH^+ are important for maintaining pmf in the WT as the gH^+ regulation relaxes. In *hope2*, the lack of
172 gH^+ regulation leads to a compensatory increase in vH^+, maintaining pmf at WT levels beyond ~150 s

173 illumination. Having established that *hope2* had WT-level pmf after 6 min of low actinic light, we next
174 investigated how *hope2* and *pgr5* behaved during increasing light intensities. This revealed that pmf in
175 the WT plateaued at ca. 0.8 at 250 µmol photons m^{-2} s^{-1} (Figure 1f), similar to previous reports
176 (Nishikawa et al., 2012; Wang et al., 2015; Yamamoto et al., 2016; Nikkanen et al., 2018; Nikkanen et
177 al., 2019; Yamamoto and Shikanai, 2020; Hepworth et al., 2021; Rühle et al., 2021) and pmf in *hope2*
178 was not significantly different at all light intensities. gH^+ and vH^+ on the other hand, were still higher in
179 *hope2* (Figure 1g and h), confirming that increased vH^+ drives the maintenance of WT levels of pmf in
180 *hope2*. On the other hand, *pgr5* had diminished pmf at all but the lowest light intensity due to a
181 combination of lower vH^+ and higher gH^+ compared to the WT (Figure 1g and h).

182 Cyclic electron transfer is upregulated in *hope2*

183 We find that increased gH^+ in *hope2* is compensated for by an increase in vH^+, which could be caused
184 by either increased LET, CET or another alternative electron flow. To test this further, we compared
185 the thylakoid proteomes for proteins that were up or downregulated in *hope2* relative to the WT
186 (Supplemental Figure S1). As expected, ATP synthase abundance was decreased by ~50% in *hope2*
187 consistent with past immunoblotting results (Takagi et al., 2017). Other proteins significantly
188 upregulated ($p < 0.05$) included the state transition kinases STN7 and STN8, PsbS, violaxanthin de-
189 epoxidase (VDE), and the H^+/K^+ antiporter KEA3, while those downregulated included TRXM2, PSAO
190 and PSBT. Most strikingly however, PGR5 (0.56-fold increase) and multiple subunits of the NDH
191 complex (ndhF, H, I, K, M, N, O, S and U) (~0.21-0.41-fold increase) showed significantly increased
192 abundance in *hope2* (Figure 2a). Interestingly however, PGRL1 was unchanged in *hope2* (Figure 2a).
193 Increased abundance in *hope2* was also seen for LFNR1 and LFNR2 and their membrane tether,
194 thylakoid rhodanese-like protein (TROL), which have been recently linked to CET (Kramer et al.,
195 2021). On the other hand, in *pgr5*, both PGRL1 isoforms and NDH subunits were decreased by ~0.70-
196 1.31 and ~0.21-0.35-fold respectively (Figure 2a), as shown previously by immunoblotting (Munekage
197 et al., 2004; Nikkanen et al., 2018; Wada et al., 2021). Given these results we hypothesized that pmf
198 may be maintained in *hope2* via increased CET relative to WT. A well-established method of assessing
199 changes in CET is the relationship between vH^+ and LET (calculated by chlorophyll fluorescence)
200 (Okegawa et al., 2005; Livingston et al., 2010a; Livingston et al., 2010b; Strand et al., 2015; Strand et
201 al., 2017). A steeper slope indicates a greater contribution of CET to vH^+. In *hope2*, the relationship
202 between vH^+ and LET was significantly ($p < 0.05$) steeper than in the WT Col-0, with a slightly
203 shallower slope observed in *pgr5* (Figure 2b). We estimate from the slope that vH^+ is decreased by 7.9%
204 in *pgr5,* similar to the 13% previously determined by this method (Avenson et al., 2005), but increased
205 by 48% in *hope2*. Deviation of a linear relationship between the quantum yields of PSI (Y(I)) and PSII
206 (Y(II)) at varying light intensities provides another indication of CET capacity (Okegawa et al., 2005;
207 Livingston et al., 2010a; Livingston et al., 2010b; Strand et al., 2015; Strand et al., 2017). Consistent

208 with higher CET in *hope2* we found increased Y(I) relative to Y(II) compared to the WT, while the
209 smallest deviation was found in *pgr5* (Figure 2c). An alternative complementary method of assessing
210 CET *in vivo* involves following the rate of P700 oxidation induced by far red (FR) light which
211 preferentially excites PSI (Joliot and Joliot, 2002; Okegawa et al., 2007; Rühle et al., 2021). In this
212 assay, decreased CET activity results in faster P700 oxidation and lower half-times ($t_{0.5}$), whereas
213 increased CET has the opposite effect (Joliot and Joliot, 2002; Joliot and Johnson, 2011; Rühle et al.,
214 2021). Consistent with lower CET in *pgr5*, FR light–induced P700 oxidation was faster than WT *gl1*
215 (Figure 2d). However, P700 oxidation $t_{0.5}$ in *hope2* was significantly ($p = 0.0200$) slower than Col-0
216 (Figure 2d), in line with increased CET relative to WT Col-0. We confirmed that these differences in
217 P700 oxidation rate could not be ascribed to differences in antenna size between the WT Col-0 and
218 *hope2* by infiltration of leaves with DCMU and methyl viologen, which eliminate donor and acceptor
219 side limitations on PSI (Supplemental Figure S2).

220

221 **PGR5 is the major CET pathway in *hope2***

222 Since both NDH and PGR5 abundance increased in *hope2* we sought to ascertain whether one or both
223 pathways contributed to the observed increases in CET and vH^+. To that end the double mutants *hope2*
224 *ndho* and *hope2 pgr5* were created and verified by DNA sequencing for the *hope2* mutation and
225 immunoblotting for NdhS, PGR5 and PGRL1 levels (Supplemental Figure S3). Previous high CET
226 mutants have involved the NDH pathway (Livingston et al., 2010a; Livingston et al., 2010b; Strand et
227 al., 2015; Strand et al., 2017), which prompted us to first analyse the *hope2 ndho* double mutant. At
228 light levels above 250 µmol photons m^{-2} s^{-1}, pmf in the *hope2 ndho* double mutant was not significantly
229 different to the *hope2* and *ndho* single mutants (Figure 3a), though both *ndho* and *hope2 ndho* showed
230 slightly lower pmf than the WT, consistent with past results (Nikkanen et al., 2018). Similarly, gH^+ and
231 vH^+ were largely unchanged in *hope2 ndho* compared to *hope2*, which were both significantly higher
232 than *ndho* and WT (Figure 3b-c). The NPQ level in the *hope2* mutant was WT-like, whereas *ndho*
233 showed higher NPQ as previously reported (Rumeau et al., 2005; Takagi et al., 2017). The *hope2 ndho*
234 mutant showed an NPQ level between *hope2* and *ndho*, demonstrating that NPQ in *hope2* does not
235 require NDH (Figure 3d), although clearly elevated NPQ in *ndho* is affected by loss of gH^+ regulation.
236 The PSII quantum yield (Y(II)) and PSII Q_A^- reduction (1-qL) were similar in *hope2 ndho* and *hope2*,
237 only low light had a moderate effect (Figure 3e-f). The PSI quantum yield (Y(I)) is increased in *hope2*
238 relative to the WT at moderate light intensities between 250 and 500 µmol photons m^{-2} s^{-1}, whereas
239 *hope2 ndho* and *ndho* were lower than WT and *hope2* at low light but was similar at higher light
240 intensities (Figure 3g). Finally, PSI donor side limitation (Y(ND)) and PSI acceptor-side limitation
241 (Y(NA)) in *hope2 ndho* were also similar to *hope2*, which were significantly lower than the WT and
242 *ndho* (Figure 3h-i). CET measured via the relationship between vH^+ and LET or Y(I) and Y(II) in *ndho*
243 was similar to WT, whereas *hope2 ndho* behaved largely like *hope2*, with only slight deviation seen at

244 the lowest LET levels (Figure 3j,k), suggesting the major contribution of the NDH pathway is in low
245 light. Furthermore, CET measured via the P700 oxidation method in *hope2 ndho* showed it was
246 unchanged compared to *hope2* ($p = 0.2424$), suggesting the elevated CET is little affected by the
247 absence of the NDH pathway under FR illumination (Figure 3l).

248 Since removal of NDH from the *hope2* background did not strongly affect the enhanced vH^+ in
249 *hope2* we next examined the effect of loss of PGR5. The Arabidopsis *pgr5* mutant has recently been
250 shown to have point mutations in two separate genes encoding the PGR5 and PPT1 proteins, the latter
251 of which seems to perpetuate long-term damage to PSI (Wada et al., 2021). Importantly for the
252 conclusions of this work, however, the low pmf and Y(ND) phenotypes were shown to be associated
253 with the PGR5 mutation alone, consistent with tDNA knock-out results in rice and a recent CRISPR-
254 Cas9 *pgr5* mutant generated in *Arabidopsis* (Nishikawa et al., 2012; Penzler et al., 2022). Pmf and vH^+
255 in the *hope2 pgr5* double mutant dropped significantly below *hope2*, except under very low light (Figure
256 4a,c), whereas gH^+ was similar in *hope2* and *hope2 pgr5* (Figure 4b). In line with this, NPQ and Y(II)
257 were lower in *hope2 pgr5* and 1-qL was higher compared to *hope2* (Figure 4d-f). Y(I) was also
258 substantially lower at all light levels in *hope2 pgr5* compared to *hope2* (Figure 4g). Y(ND) remained
259 low in the *hope2 pgr5* double mutant, similar to the respective single mutants (Figure 4h) and Y(NA)
260 in *hope2 pgr5* was similar to *pgr5* and elevated with respect to *hope2* (Figure 4i). CET measured via
261 the relationship between vH^+ and LET or Y(I) and Y(II) was significantly less steep ($p=0.008$) in *hope2*
262 *pgr5* compared to *hope2* and resembled WT (Figure 4j, k). In line with this, FR-induced P700 oxidation
263 in *hope2 pgr5* was also much faster than in *hope2*, indicating that the increased CET is abolished and
264 consistent with this the $t_{0.5}$ was significantly lower than *hope2* ($p<0.0001$) (Figure 4l). Overall, these
265 data show that in *hope2*, PGR5-dependent CET is required to maintain WT-level pmf by increasing
266 vH^+, whereas NDH-dependent CET only makes a substantial contribution to pmf in the *hope2*
267 background at lower light intensities. We verified this furthermore by growing genotypes under control
268 and high light conditions. This showed that plant rosette area and fresh weight were significantly
269 impaired in *hope2 pgr5* but to a lesser extent in *hope2 ndho* (Figure S4). Furthermore, Fv/Fm in *pgr5*
270 and *hope2 pgr5* was significantly impaired after high light treatment.

271

272 **Photosynthetic control is absent in *hope2* despite maintenance of WT levels of ΔpH**

273 The maintenance of WT levels of pmf in *hope2* due to increased PGR5-dependent CET raised the
274 question of why NPQ is WT-like, while Y(ND) is *pgr5*-like? One possibility is that the pmf is
275 differently partitioned between the ΔpH and ΔΨ components in *hope2,* which given the differing
276 reported sensitivity of NPQ and Y(ND) to ΔpH might explain their contrasting responses (Horton et al.,
277 1991; Nishio and Whitmarsh, 1993). Indeed, our proteomic data shows an increase in the relative
278 abundance of the putative H^+/K^+ thylakoid antiporter KEA3, which could modify the ΔpH/ΔΨ

279 partitioning of pmf in this mutant (Supplemental Figure S1). To test these ideas further we first
280 confirmed that NPQ in *hope2* was of the ΔpH-dependent rapidly-relaxing qE type rather than
281 photoinhibitory or sustained qI-type quenching (Supplemental Figure S5). Next, we utilized the ECS
282 partition method to assess the relative ΔpH and ΔΨ contributions to pmf. Previous ECS partitioning
283 data suggested *hope2* may have a slightly lower ΔpH contribution to pmf (Takagi et al., 2017).
284 However, this method has recently been called into question due to the overlapping absorption changes
285 associated with qE which lead to overestimation of ΔΨ contributions to pmf, particularly when
286 zeaxanthin synthesis is incomplete (Wilson et al., 2021). We thus compared using the partition method
287 the pmf composition under conditions where zeaxanthin synthesis was incomplete (increasing light
288 intensity every 20 seconds) versus complete (decreasing light intensity following 10 minutes
289 illumination at 1421 µmol photons m^{-2} s^{-1}). The results showed that pmf takes longer to establish in
290 *hope2* consistent with the data in Figure 1c, as a result the apparent ΔΨ contribution to pmf is larger in
291 *hope2* than in the WT (Figure 5a, b). By contrast, once pmf is established after 10 minutes of high light
292 little difference in either the extent of pmf or the relative ΔΨ versus ΔpH contribution was observed
293 between *hope2* and the WT (Figure 5b, c). In line with this, while NPQ is smaller in *hope2* during
294 induction compared to the WT, once pmf is fully established in *hope2* NPQ reaches WT levels (Figure
295 5d). Yet, in spite of this Y(ND) remains much smaller and Y(NA) much larger in *hope2* (Figure 5e,f).
296 Therefore, lower Y(ND) in *hope2* cannot be ascribed to lower ΔpH contribution to pmf.

297

298 **Discussion**

299 ***hope2* is able to maintain CO_2 assimilation through increased CET**

300 Proton motive force is harnessed for the production of ATP by ATP synthase, while its major ΔpH
301 component also plays an important regulatory role triggering qE and Y(ND). *Hope2*, a recently
302 described G134D γ1-subunit mutant in Arabidopsis was particularly interesting because it showed a
303 similar phenotype compared to *pgr5* with respect to the loss of photosynthetic control and high gH^+ but
304 key differences with respect to qE and CO_2 assimilation (Munekage et al., 2004; Takagi et al., 2017).
305 Thus, ATP synthase regulation and CET may play distinct roles in the regulation of photoprotection
306 and ATP/NADPH balance. Here we show that despite high gH^+, *hope2* is able to maintain pmf at WT
307 levels through increased vH^+. The normal pmf levels we observe in *hope2* are a key point of difference
308 with the previous study by Takagi *et al*., (2017). In this previous study pmf was more variable, being
309 lower than WT under low O_2 or ambient CO_2 without pre-illumination and similar following pre-
310 illumination. We found these differences could be explained by the slower establishment of pmf in
311 *hope2* (Figs 1c, d, 5a). Comparison of the respective quantum yields of PSI and PSII showed increased
312 electron transfer rate through PSI in *hope2* compared to WT consistent with enhanced CET
313 (summarized in Figure 6). CET is notoriously difficult to measure owing to the fact that it produces no

314 net product and utilizes a common set of spectroscopically active-redox carriers with LET. Nonetheless,
315 careful comparison of vH^+ with the rate of LET demonstrates a steeper relationship in *hope2*, consistent
316 with the phenotype seen in other high CET mutants previously described (Livingston et al., 2010a;
317 Livingston et al., 2010b; Strand et al., 2015; Strand et al., 2017). A complementary method for assessing
318 CET involves illumination monitoring the rate of P700 oxidation with FR. Consistent with the vH^+/LET
319 method the FR oxidation of PSI is slower in *hope2* confirming an increased rate of CET. The slower
320 establishment of pmf in *hope2* (Figure 1c,d) seems to reflect the varying timescales for relaxation of
321 ATP synthase and activation of CET. Thus, in the first few moments following illumination increases
322 in pmf depend largely on the restricted gH^+ in the WT. As the ATP synthase regulatory γ1-subunit thiol
323 becomes gradually reduced in the light gH^+ increases (Konno et al., 2012). Following this increase in
324 gH^+, vH^+ must be increased if pmf is to be maintained. The maintenance of WT-levels of pmf likely
325 explains the similar CO_2 assimilation rates in *hope2* compared to the WT and is further evidence for an
326 important role of CET in ensuring the optimal ATP/NADPH ratio.

327

328 **Enhanced CET in *hope2* depends on the PGR5-dependent rather than NDH-dependent pathway**

329 A proteomic comparison of the thylakoid membranes from *hope2* and WT plants showed that NDH and
330 PGR5 abundance was upregulated. We therefore constructed the double mutants *hope2 pgr5* and *hope2*
331 *ndho,* to understand the respective contributions of the two pathways to increased CET in *hope2*. The
332 steeper vH^+ versus LET and Y(I) versus (YII) slopes and slower FR-driven P700 oxidation seen in
333 *hope2* were lost in *hope2 pgr5* double mutant, and it suffered from the more extreme PSI acceptor side
334 limitation (Y(NA)) seen in *pgr5*. By contrast, the phenotype of the *hope2 ndho* double mutant was less
335 dramatic, with a similar rate of P700 oxidation to *hope2*, with only a slight decrease in the vH^+/LET
336 slope seen at low light and although there was an increase in Y(NA) compared to *hope2* this was less
337 severe than in *hope2 pgr5*. The predominant reliance of *hope2* on the PGR5-dependent CET1 pathway
338 is key point of difference compared to other previously characterized high cyclic electron flow (*hcef*)
339 mutants, which use the NDH-dependent CET2 pathway (Livingston et al., 2010a; Livingston et al.,
340 2010b). The factors regulating CET1 and CET2 have yet to be fully elucidated (Yamori and Shikanai,
341 2015; Yamori et al., 2016), though H_2O_2 signaling and $NADPH/NADP^+$ redox balance have been
342 recently implicated in control of the NDH and PGR5 pathways, respectively (Strand et al., 2015; Strand
343 et al., 2016). However, since Y(NA) is high in *hope2,* both signals would be expected, consistent with
344 the increased abundance of both PGR5 (0.56-fold increase) and NDH subunits (0.21-0.41-fold increase)
345 we find in this mutant. By contrast, quantification of NDH levels by immunoblotting in *hcef1* revealed
346 a 15-fold increase in NDH and a 50% decrease in PGR5 (Livingston et al., 2010a). Comparison of
347 *hope2* and *hcef1* reveals a large difference in gH^+ between the mutants. Therefore, if pmf can be restored
348 by combination of ATP synthase gH^+ downregulation and increases in NDH-dependent CET2, it may
349 negate the need for upregulation of PGR5. It may be important in this regard that we see the greatest

350 contribution of the NDH-pathway (H^+/e^- ratio of 4) in *hope2* under low light, where it is less
351 thermodynamically limited by backpressure from the pmf (Strand et al., 2017). This is in line with
352 previous work showing *ndho* and *crr* mutants show more substantial phenotypes in low light situations
353 (Yamori et al., 2011; Wang et al., 2015; Yamori et al., 2015; Yamori and Shikanai, 2015). By contrast,
354 the lower efficiency PGR5 pathway (H^+/e^- ratio of 2) may be preferred in high light, consistent with the
355 stronger phenotype of *pgr5* plants under such conditions (Munekage et al., 2004). Therefore, a
356 combination of simple competition for excess electrons at the PSI acceptor side and thermodynamic
357 constraints on turnover may determine which CET pathway is favored in particular circumstances.
358 Irrespective, the isolation of a high CET mutant that depends on PGR5 is important since the steady-
359 state contribution of CET1 is generally estimated to be low (<13% of LET) and difficult to measure.
360 *Hope2* is therefore a useful tool for future research on PGR5-dependent CET1.

361

362 **High CET in the absence of ATP synthase regulation fails to restore photosynthetic control**

363 Previously, repetitive flash treatment showed that PSI in *hope2* was, similar to *pgr5*, susceptible to
364 photoinhibition (Takagi et al., 2017). However, it was unclear whether the *pgr5* phenotype was
365 primarily due to loss of gH^+ control or loss of CET1 (Avenson et al., 2005; Yamamoto and Shikanai,
366 2020). While the maintenance of WT-levels of pmf through enhanced CET in *hope2* allowed normal
367 qE-levels to develop, Y(ND) remained virtually absent (summarized in Figure 6). *Prima facie* this
368 suggests that gH^+ regulation of ATP synthase is crucial for photosynthetic control. Accordingly, even
369 strongly enhanced PGR5-dependent CET1 does not protect against PSI photoinhibition in *hope2*. The
370 failure of CET to protect PSI is consistent with recent results showing that both CET1 and CET2 do not
371 act as photoprotective electron sinks in the absence of other mechanisms of acceptor side regulation of
372 PSI (Rantala et al., 2020). Since photosynthetic control relies on the low lumenal pH-induced slow
373 down of PQH_2 oxidation by the Rieske iron-sulphur protein of cytb_6f (Nishio and Whitmarsh, 1993;
374 Jahns et al., 2002), the most logical explanation for loss of Y(ND) is a loss of ΔpH in *hope2*. Previously,
375 a difference in relative partitioning of pmf into ΔΨ and ΔpH compared to the WT was found in *hope2*
376 (Takagi et al., 2017). However, we traced these apparent differences in partitioning to a slower
377 establishment of pmf in *hope2,* which leads to increased overlap with the qE related absorption changes
378 as described for the *npq1* mutant lacking zeaxanthin (Wilson et al., 2021). Once pmf is established in
379 *hope2,* and presumably zeaxanthin synthesis is completed, then no major differences in the amplitude
380 of ΔpH between *hope2* and the WT are present. Therefore, changes in ΔpH are not the cause of the low
381 photosynthetic control phenotype in *hope2*. These data mirror similar reports in *pgr5* plants
382 overexpressing the *Chlamydomonas reinhardtii* plastid terminal oxidase 2 (PTOX2) protein and the
383 FNR antisense mutant of *Nicotiana benthamiana* , both of which showed normal qE but lacked
384 photosynthetic control (Hald et al., 2008; Zhou et al., 2022). One possibility is that just the relationship
385 between qE and ΔpH is modified by the xanthophyll cycle de-epoxidation state (Rees et al., 1989;

386 Horton et al., 1991), so the relationship between Y(ND) and ΔpH is regulated by NADPH/NADP$^+$ redox
387 poise (Johnson, 2003; Hald et al., 2008). In *hope2* where Y(NA) is high, NADPH/NADP$^+$ redox poise
388 is likely disturbed. The fact that Y(ND) can be restored in *pgr5* in the presence of the artificial PSI
389 electron acceptor methyl viologen (Munekage et al., 2002; Wang et al., 2018) or via transgenic
390 expression of *Physcomitrium patens* Flv proteins (Yamamoto et al., 2016) could be interpreted as
391 further evidence for this hypothesis. Further work is now required to test these ideas.

392

393 **The nature of the mis-regulation of ATP synthase in *hope2***

394 The nature of the mis-regulation of ATP synthase in *hope2* remains unclear. Previously Takagi et al.,
395 (2017) showed that gH$^+$ in *hope2* fails to respond to CO_2 concentration suggesting either metabolic
396 control may be lost in this mutant or that the mutant enzyme is less efficient than the WT version. The
397 mechanism of metabolic control of the ATP synthase is still unclear, though gH$^+$ is known to be
398 sensitive to Pi, NADPH/NADP$^+$ redox poise in addition to CO_2 concentration suggesting it is able to
399 sense the stromal metabolism and so tune ATP production accordingly (Velthuys, 1978; Kanazawa and
400 Kramer, 2002; Avenson et al., 2005; Takizawa et al., 2008; Kohzuma et al., 2013). The G134D mutation
401 in the γ1-subunit of *hope2* ATP synthase is in the GxxGxxG NADP(H)-binding motif of the Rossman
402 fold domain. This motif of the γ1-subunit is conserved in ATP synthases from chloroplasts and
403 cyanobacteria (GxxGxxG), mitochondria (TxxGxxG) and *E. coli* (SxxGxxG), (Figure S6) although its
404 function remains unknown. Given the previous demonstration that NADPH/NADP$^+$ redox poise can
405 affect the gH$^+$ of the ATP synthase in *Chlamydomonas* (Velthuys, 1978), one possibility is that the
406 Rossman fold is the site of metabolic regulation of the ATP synthase complex. However, several of our
407 observations are more closely aligned with the leak hypothesis. Firstly, we observe that gH$^+$ starts at a
408 higher value during the dark to light transition in *hope2* suggesting the mutant enzyme is affected in
409 both its oxidized and reduced states (Figure 1d). Secondly, if high gH$^+$ in *hope2* were producing a higher
410 ATP/ADP ratio in *hope2* compared to the WT one would expect that it would increase the capacity for
411 CO_2 assimilation under high CO_2 conditions, something which we do not observe (Figure 1b). Rather
412 our data suggest that *hope2* is having to 'peddle faster' to obtain the WT ATP/ADP ratio via increasing
413 CET, as discussed above. Indeed, the C87K mutation in the Rossman fold motif of the *E. coli* ATP
414 synthase γ-subunit (C139 in Arabidopsis) has been shown to decrease the coupling efficiency between
415 the Fo rotor and F1 head, increasing the effective H$^+$/ATP ratio (Li et al., 2019). Therefore, the G134D
416 mutation in close proximity to this region of the protein could produce a similar effect in Arabidopsis.

417

418 **Conclusions**

419 Our data have clarified the respective importance of proton influx and efflux control in
420 photosynthetic regulation. We found ATP synthase gH$^+$ regulation is indispensable for photosynthetic

421 control, even when CET can maintain pmf to ensure an optimal ATP/NADPH ratio and qE. This work
422 highlights the interconnectedness and mutual dependence of the various photoprotective regulatory
423 mechanisms in addition to the remarkable ability of the photosynthetic apparatus to preserve pmf via
424 molecular plasticity in thylakoid protein composition.

425

426

427

428

429

430 Materials and Methods

431

432 **Plant material, growth conditions, generation of double crosses and growth experiment**

433 *Arabidopsis thaliana* mutants *hope2* and the WT background Col-0 and *pgr5* and the WT background
434 *gl1* were grown in a controlled-environment chamber for at least 6 weeks at 21/15°C day/night, 60%
435 rel. humidity with an 8-hour photoperiod at a light intensity of 200 µmol photons m^{-2} s^{-1}. Double mutants
436 were generated by crossing *hope2* with either *pgr5* or *ndho*. Seeds from successful crosses were sown
437 and allowed to self-fertilize. Seedlings were screened for the *pgr5* phenotype using an Imaging PAM
438 (Heinz Walz GmbH, Effeltrich, Germany). Plants with low NPQ were then screened for the high gH^+
439 phenotype, characteristic for *hope2*, using the Dual PAM (Heinz Walz GmbH, Effeltrich, Germany).
440 Crosses displaying both phenotypes were used for thylakoid isolation (described below). Western blots
441 were performed on isolated thylakoids using the NdhS (AS164066, 1:5,000 dilution) and PGR5
442 (AS163985, 1:1,300 dilution) antibodies (all purchased from Agrisera, Vännäs, Sweden).
443 Homozygosity for *hope2* was verified by Sanger sequencing, using the primers 5'-
444 ACTTCCTCACCTCCTTCACG-3' and 5'-AATTTCCCTTCTTGCCCACG-3'. For the growth
445 experiment, 12 biological replicates of each genotype were randomly distributed in a 4x6 seed tray for
446 control and high light treatment. After three weeks in control conditions, the first rosette area
447 measurement was taken. Half of the trays were then transferred to medium light (400 µmol photons m^{-}
448 ^{2} s^{-1}) for one week. Plants were then shifted to high light (685 µmol photons m^{-2} s^{-1}) for 18 days. At the
449 end of the growth experiment (day 24), a subset of plants of each genotype and growth light was used
450 for Fv/Fm determination and fresh weight of all plants was determined as well. Rosette areas were
451 measured using the iDIEL Plant Software (Dobrescu et al., 2017).

452 **Chlorophyll fluorescence and *in situ* P700 absorption spectroscopy**

453 A Dual-KLAS-NIR photosynthesis analyzer (Heinz Walz GmbH, Effeltrich, Germany) was used for
454 pulse-amplitude modulation chlorophyll fluorescence measurements and P700 absorption spectroscopy
455 in the near-infrared (Klughammer and Schreiber, 2016; Schreiber and Klughammer, 2016). After plants
456 had dark-adapted for at least 1 h, four pairs of pulse-modulated NIR measuring beans were zeroed and
457 calibrated before each measurement. For each genotype, one leaf was used to generate differential
458 model plots according to manufacturer's protocol, which were used for online deconvolution to
459 determine redox changes of P700. Prior to each measurement, maximum oxidation of P700 was
460 determined by using the pre-programmed NIRmax routine. This consisted of a 3 s pulse of 635 nm
461 actinic light on top of which a 30 ms multiple turnover flash (MT) was given after 800 ms, followed by
462 4 s of darkness and 10 s of 255 µmol photons m^{-2} s^{-1} 740 nm FR light and a MT at the end to achieve
463 full oxidation of P700. NIRmax values were determined by using the pre-programmed "Get Max-
464 Values" option. Dark-fluorescence (Fo) and maximal fluorescence (Fm) were determined prior to light
465 or induction curves. Photosynthetic parameters were determined by using measuring beam intensities
466 of 20 µmol photons m^{-2} s^{-1} and 14 µmol photons m^{-2} s^{-1} for chlorophyll fluorescence and P700 redox
467 changes, respectively and a 18,000 µmol photons m^{-2} s^{-1} saturating pulse. Photosynthetic parameters
468 were calculated as follows: Y(II) = (Fm'-F)/Fm', NPQ = (Fm-Fm')/Fm', Y(I) = (Pm'-P)/Pm, Y(NA) =
469 (Pm-Pm')/Pm, Y(ND) = $(P-P_0)$/Pm. For light curves, measurements were taken after 5 min at each light
470 intensity. For induction curves, AL intensity was set to 169 µmol photons m^{-2} s^{-1} and measurements
471 were taken at multiple time points after AL was turned on. To determine P700 oxidation for CET
472 determination, leaves were exposed to a weak measuring light for 30 s, followed by a MT. FR light was
473 then turned on for 20 s. Half-time of P700 oxidation was determined by fitting an allosteric sigmoidal
474 function (Graphpad Prism, 9.1.1).

475

476 **Electrochromic shift measurements**

477 Electrochromic shift was measured using a Dual-PAM analyzer with a P515/535 emitter/detector
478 module (Heinz Walz GmbH, Effeltrich, Germany) (Klughammer et al., 2013). Plants were dark-adapted
479 for at least 1 h prior to measurements. Proton motive force (pmf) was calculated from the decay of the
480 P515 signal when 635 nm AL was turned off, by fitting a single exponential decay to the first 300 ms
481 in the dark to determine the span of the signal decay (ECS_t). pmf was normalized by dividing ECS_t by
482 the magnitude of a 50 µs ST flash applied prior to account for leaf thickness and chloroplast density
483 (Takizawa et al., 2007; Livingston et al., 2010a; Wang et al., 2015; Takagi et al., 2017). The proton
484 conductance gH^+ was calculated as the inverse of the decay time constant τ_{ECS} of the single exponential
485 decay and proton flux was calculated as vH^+= pmf x gH^+ (Baker et al., 2007).

486

487 **Leaf infiltration**

488 Dark-adapted leaves were vacuum-infiltrated with 30 µM DCMU and 100 µM methyl viologen
489 buffered in 20 mM Hepes - pH 7.5, 150 mM sorbitol and 50 mM NaCl. Leaves were dark-adapted for
490 10 min between infiltration and measurements.

491 **Gas exchange**

492 CO_2-response (ACi) and light-response curves (AQ) were measured using the infrared gas analyser
493 system 6400-XT (LiCOR Biosciences, Lincoln, NE, USA). Prior to measurements, plants were exposed
494 to 400 ppm reference CO_2, 1500 µmol photons m^{-2} s^{-2} light at 25°C and ca. 50% relative humidity for
495 at least 10 min until steady state was reached and stomata were wide open with a Ci/Ca of >0.7. For
496 ACi curves, data was logged at various CO_2 concentrations after 90-120 s using the following sequence
497 of reference CO_2 concentrations, as recommended by (Busch, 2018): 400, 350, 300, 250, 200, 150, 100,
498 50, 400, 400, 450, 500, 650, 800, 1000, 1250. For AQ curves, sample CO_2 was set to 390 ppm and data
499 was logged after a minimum of 3 min at each light intensity, using the following sequence of light
500 intensities: 1500, 1000, 750, 500, 300, 200, 150, 50, 25, 10, 0. Reference and sample analyzers were
501 matched prior to logging the data. Maximum Rubisco activity (Vc,max) and maximum electron
502 transport rate used in RuBP regeneration (Jmax) were fitted using the FvCB model and the Plantecophys
503 package in R (Duursma, 2015).

504

505 **Thylakoid isolation**

506 Thylakoids were isolated from Arabidopsis plants 2-3 hours into the photoperiod. Plants were blended
507 in ice-cold medium containing 50 mM sodium phosphate pH 7.4, 5 mM $MgCl_2$, 300 mM sucrose and
508 10 mM NaF. The homogenate was then filtered twice through two layers of muslin cloth. The filtrate
509 was then centrifuged for 15 min at 3750 rpm at 4°C. The chloroplast pellets were then resuspended in
510 5 mM $MgCl_2$, 10 mM Tricine pH 7.4 and 10 mM NaF. After 1 min on ice, a medium containing 5 mM
511 MgCl2, 10 mM Tricine pH 7.4, 400 mM sucrose and 10 mM NaF was added. The broken chloroplasts
512 were centrifuged for 15 min at 3750 rpm at 4°C, and thylakoid pellets were resuspended in 10 mM
513 sodium phosphate pH 7.4, 5 mM MgCl2, 5 mM NaCl and 100 mM sucrose. Resuspended thylakoids
514 were centrifuged again, and pellets were resuspended in 1 mL of the same medium.

515

516

517 **Quantitative proteomic analysis of thylakoid membranes**

518 Thylakoid membrane proteins were solubilized and digested with a combination of endoproteinase Lys-
519 C and trypsin in 1% (w/v) sodium laurate, 100 mM triethylammonium bicarbonate pH 8.5 with
520 additional sample processing and analysis by nano-flow liquid chromatography-mass spectrometry as

521 previously described (Flannery et al., 2021). MaxQuant v. 1.6.3.4 (Cox and Mann, 2008) was used for
522 mass spectral data processing and protein identification with the iBAQ (Schwanhäusser et al., 2011)
523 label-free quantification option selected and other parameters as previously specified (Flannery et al.,
524 2021). iBAQ abundance scores subjected to statistical analysis using a modified Welch's t-test as
525 implemented in Perseus v. 1.6.2.3 Protein identification and label-free quantification were performed
526 using the MaxLFQ algorithm embedded within FragPipe (v. 16.0) (Yu et al., 2021). The 'match-
527 between-runs' option was selected and all other parameters were as per default. Total intensities were
528 normalized against the sum of all identified proteins. Not all proteins were identified by mass
529 spectrometry, therefore only proteins where >75% of replicates were identified were selected. The
530 normal distribution of data was verified in MaxQuant (Cox and Mann, 2008), imputed and log2
531 transformed. This data was then expressed as fold-change relative to WT, where $p < 0.05$ was
532 significantly different. The proteomics data have been deposited to the ProteomeXchange Consortium
533 via the PRIDE partner repository (http://proteomecentral.proteomexchange.org) with the dataset
534 identifier PXD033007.

535

536 **Statistical analysis**

537

538 Statistical analysis was performed using Graphpad Prism, 9.1.1, using a two-sided t-test (alpha = 0.05)
539 and the Tukey HSD test (alpha = 0.05) in R. The asterisks always indicate significant differences
540 between the Col-0 & *hope2* and *gl1* & *pgr5* or light treatments. Different letters indicate significant
541 differences.

542

543

544

545 **Accession Numbers**

546 Sequence data from this article can be found in the GenBank/EMBL data libraries under accession
547 numbers AJ245502 (hope2/ATPC1), AY060546 (PGR5), BT000905 (PGRL1), AY143808 (NDHO)

548

549

550 **Supplemental Data**

551 **Supplemental Figure S1.** Abundance of photosynthetic proteins.

552 **Supplemental Figure S2**: Determination of PSI antenna size in Col-0 and *hope2*.

553 **Supplemental Figure S3**: Verification of homozygosity of double crosses.

554 **Supplemental Figure S4**: Growth of genotypes under control and high light conditions.

555 **Supplemental Figure S5**: Determination of rapidly relaxing NPQ (qE).

556 **Supplemental Figure S6**: Sequence alignment of Rossmann fold from various organisms and

organelles.

Funding Information

M.P.J. and S.A.C. acknowledge funding from the Leverhulme Trust grant RPG-2019-045.

Acknowledgements

We would like to thank Prof. Toshiharu Shikanai for the gift of *pgr5* seeds, Prof. Chikahiro Miyake for the gift of *hope2* seeds and Prof. Eva-Mari Aro for *ndho* seeds. For the purpose of open access, the author has applied a Creative Commons Attribution (CC BY) license to any Author Accepted Manuscript version arising.

Figure Legends

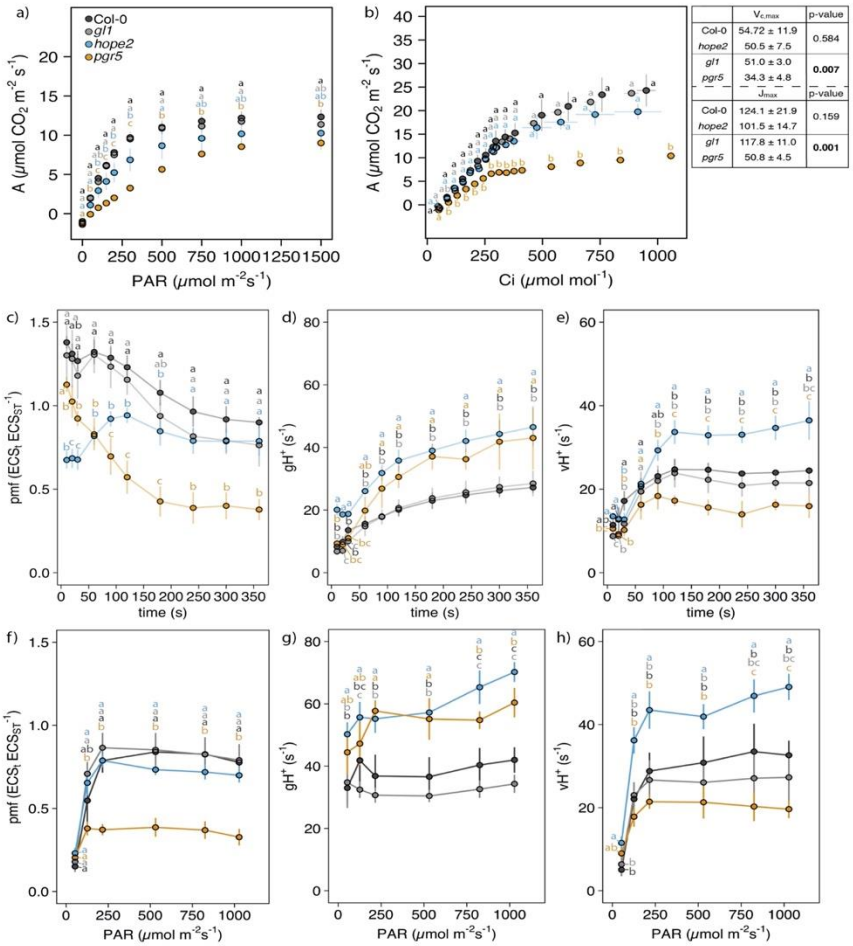

	$V_{c,max}$	p-value
Col-0	54.72 ± 11.9	0.584
hope2	50.5 ± 7.5	
gl1	51.0 ± 3.0	**0.007**
pgr5	34.3 ± 4.8	
	J_{max}	p-value
Col-0	124.1 ± 21.9	0.159
hope2	101.5 ± 14.7	
gl1	117.8 ± 11.0	**0.001**
pgr5	50.8 ± 4.5	

Figure 1: Gas-exchange and ECS measurements of WT, *hope2* and *pgr5*. a) CO_2-assimilation at various light intensities. Plants were adapted to 400 ppm reference CO_2 and 1500 µmol photons m^{-2} s^{-1} light for at least 10 min until steady-state was reached. Light levels were decreased stepwise, and data logged

after at least 3 min at each light intensity. b) CO_2-assimilation at various Ci concentrations. Plants were adapted to 400 ppm reference CO_2 and 1500 µmol photons m^{-2} s^{-1} light for at least 10 min until steady-state was reached. Reference CO_2 was decreased to 50 ppm, increased to 400 ppm and finally increased to 1250 ppm. Data was logged after 90 – 120 s at each CO_2 concentration. Table: Maximum Rubisco activity ($V_{c,max}$) and maximum electron transport rate used in RuBP regeneration (J_{max}). c, f) proton motive force (pmf); d, g) proton conductance of ATP synthase (gH^+); e, h) proton flux (vH^+). c-e) Measurements were taken during photosynthetic induction at the indicated time points using 169 µmol photons m^{-s} s^{-1} actinic light. f-h) Measurements were taken after 5 min at each indicated light intensity. Data points represent the average of 3-7 biological replicates ± SD. Colors represent genotypes analysed: Col-0 (black), *gl1* (grey), *hope2* (blue) and *pgr5* (orange). Different letters indicate statistical significance between genotypes at each time point, light intensity or Ci, calculated from a Tukey HSD test, alpha = 0.05. Bold p-values in (b) indicate significantly different $V_{c,max}$ and J_{max} between Col-0 and *hope2*, calculated from a two-sided t-test, alpha = 0.05.

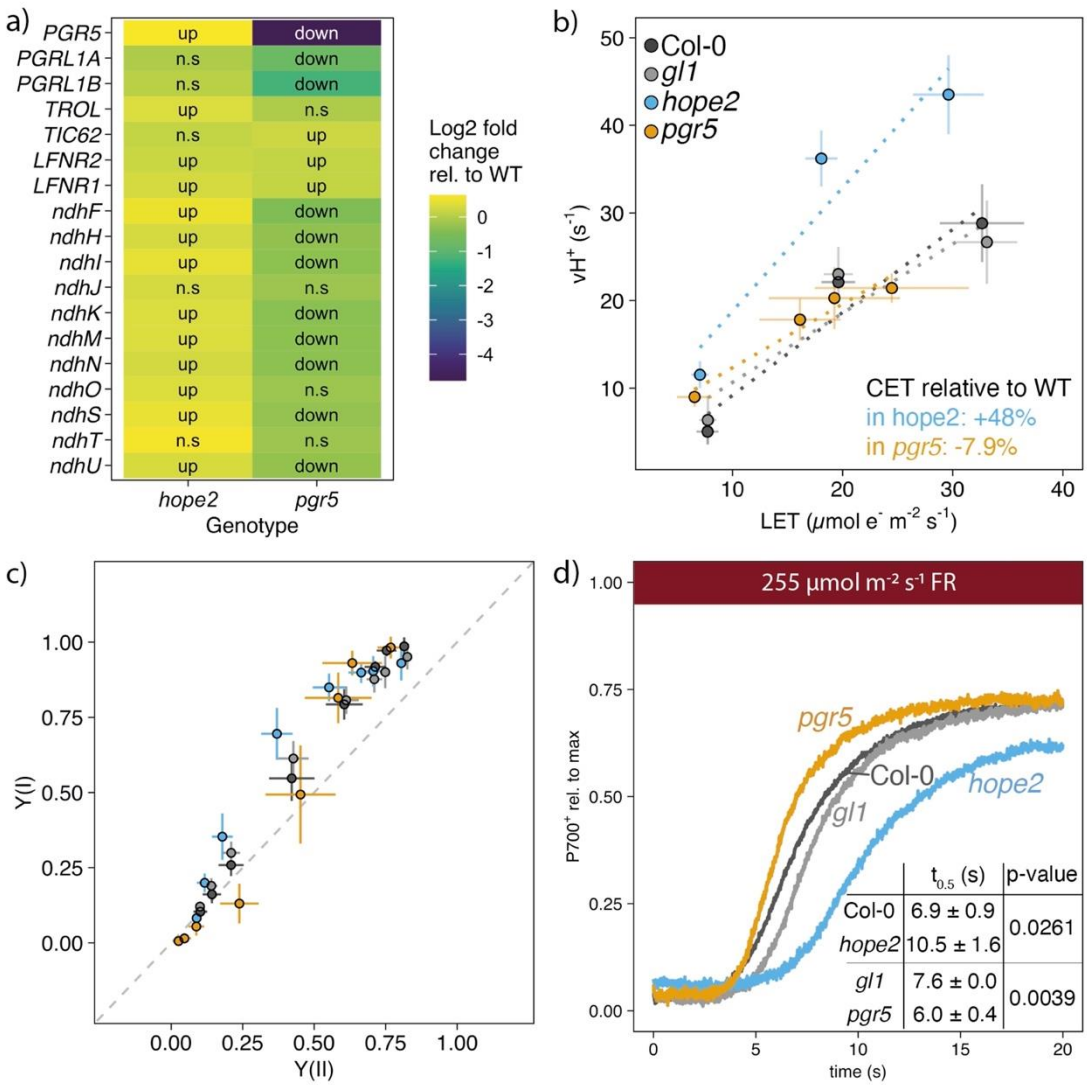

588 **Figure 2**: Measurements of cyclic electron transfer. a) Abundance of proteins involved in CET,
589 normalized to WT. b) Proton flux vs. linear electron transfer. Higher flux at similar LET indicates
590 increased cyclic electron transfer. c) Yield of photosystem I vs. yield of photosystem II. d) P700
591 oxidation during FR light. Prior to FR light, leaves were exposed to a weak ML for 30 s, followed by a
592 SP and 30 s of darkness. Data was normalized to maximal P700 oxidation after 30 s FR light and a SP.
593 Insert: Half-life of P700 oxidation determined by fitting an allosteric sigmoidal function prior to the SP.
594 Data points represent the average of 3-6 biological replicates ± SD. Colors represent genotypes
595 analyzed: Col-0 (black), *gl1* (grey), *hope2* (blue) and *pgr5* (orange). Different letters indicate statistical
596 significance between genotypes at each time point, calculated from a Tukey HSD test, alpha = 0.05. In
597 (a) "Up" refers to significantly ($p<0.05$) more abundant proteins and "down" significantly ($p>0.05$) less
598 abundant proteins, "n.s." = not significant.

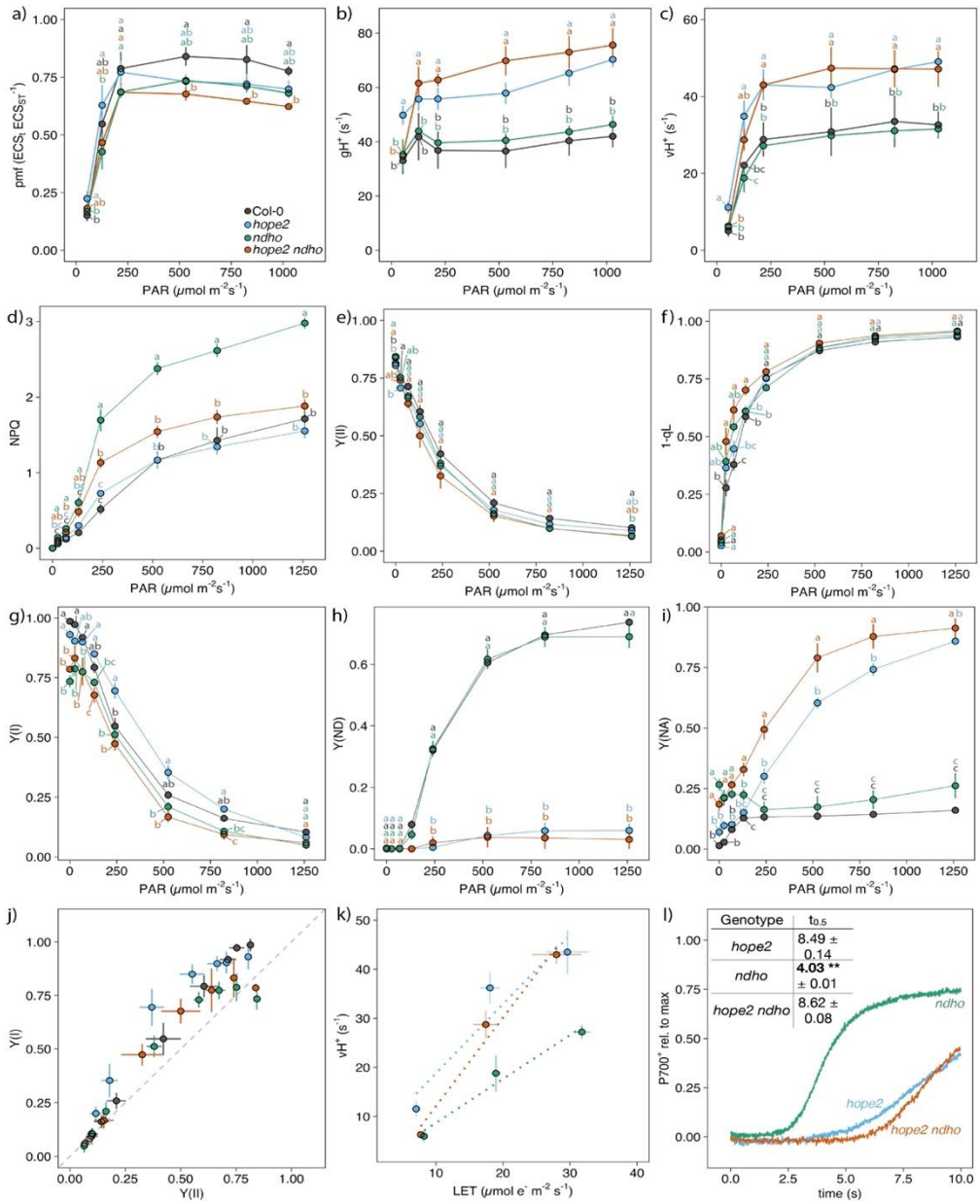

599

Figure 3: Photosynthetic parameters and CET measurements in *hope2 ndho*. a) proton motive force (pmf). b) proton conductance of ATP synthase (gH^+). c) proton flux (vH^+). d) nonphotochemical fluorescence quenching (NPQ). e) quantum yield of photosystem II (Y(II)). f) 1-qL (PSII acceptor-side limitation). g) quantum yield of photosystem I (Y(I)); h) donor-side limitation of PSI (Y(ND)). i) acceptor-side limitation of PSI (Y(NA)). j) Y(I) vs. Y(II). k) Proton flux vs. linear electron transfer. l) P700 oxidation during FR light, insert: $t_{0.5}$ (s). Data points represent the average of 3-6 biological replicates ± SD. Colors represent genotypes analyzed: Col-0 (black), *hope2* (blue), *ndho* (green) and *hope2 ndho* (red). Different letters indicate statistical significance between genotypes at each light intensity, calculated from a Tukey HSD test, alpha = 0.05. Asterisks in (k) and (l) indicate $p<0.001$ calculated from a one-way ANOVA of slopes or $t_{0.5}$ between either *hope2* and *ndho* or *hope2 ndho*. N.s. indicates "not significant".

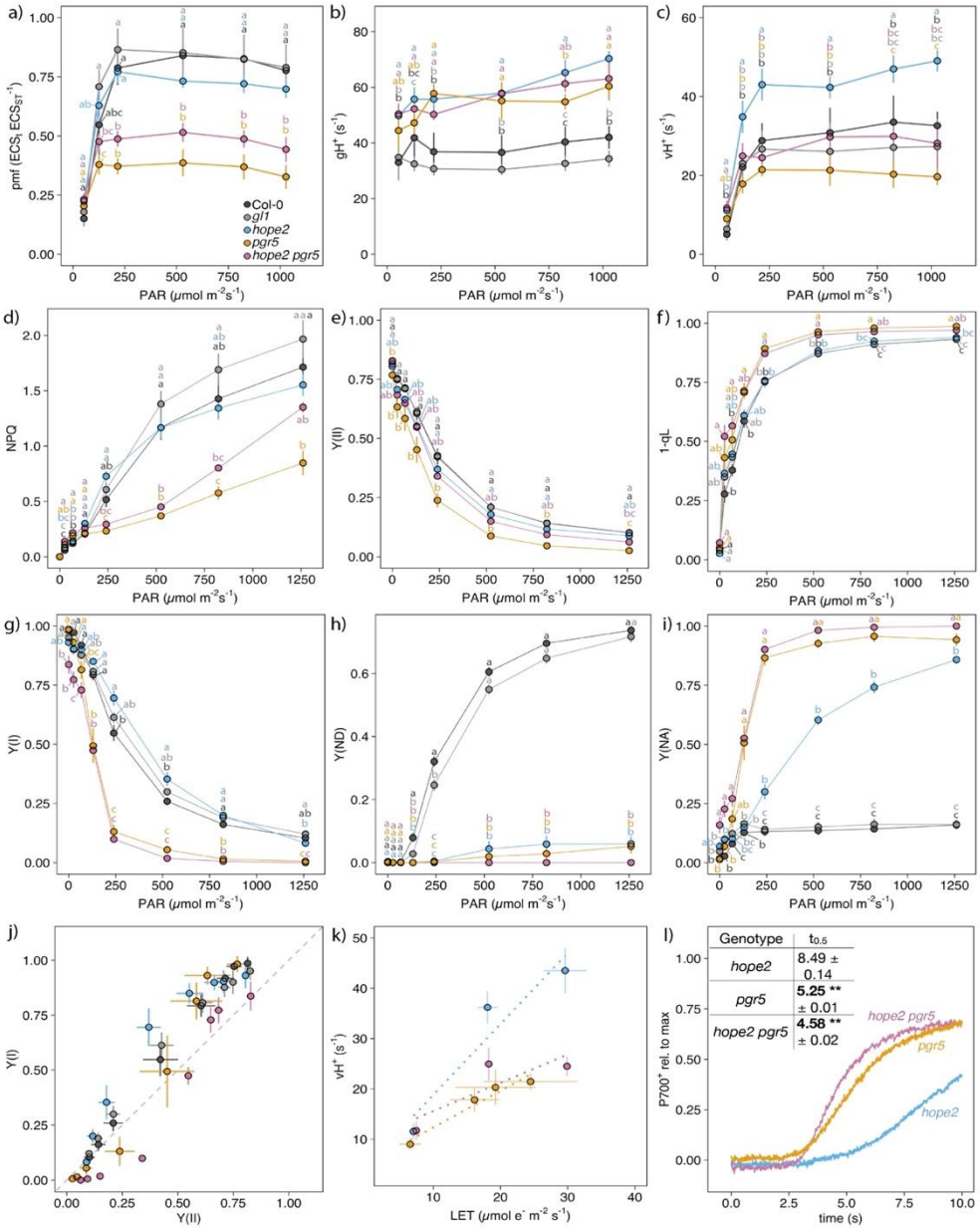

612 **Figure 4**: Photosynthetic parameters and CET measurements in *hope2 pgr5*. a) proton motive force
613 (pmf). b) proton conductance of ATP synthase (gH^+). c) proton flux (vH^+). d) nonphotochemical
614 fluorescence quenching (NPQ). e) quantum yield of photosystem II (Y(II)). f) 1-qL (PSII acceptor-side
615 limitation). g) quantum yield of photosystem I (Y(I)); h) donor-side limitation of PSI (Y(ND)). i)
616 acceptor-side limitation of PSI (Y(NA)). j) Y(I) vs. Y(II). k) Proton flux vs. linear electron transfer. l)
617 P700 oxidation during FR light, insert: $t_{0.5}$ (s). Data points represent the average of 3-6 biological
618 replicates ± SD. Colors represent genotypes analyzed: Col-0 (black), *gl1* (grey), *hope2* (blue), *pgr5*
619 (orange) and *hope2 pgr5* (pink). Different letters indicate statistical significance between genotypes at
620 each light intensity, calculated from a Tukey HSD test, alpha = 0.05. Asterisks in (k) and (l) indicate
621 $p<0.001$ calculated from a one-way ANOVA of slopes or $t_{0.5}$ between either *hope2* and *pgr5* or *hope2*
622 *pgr5*.

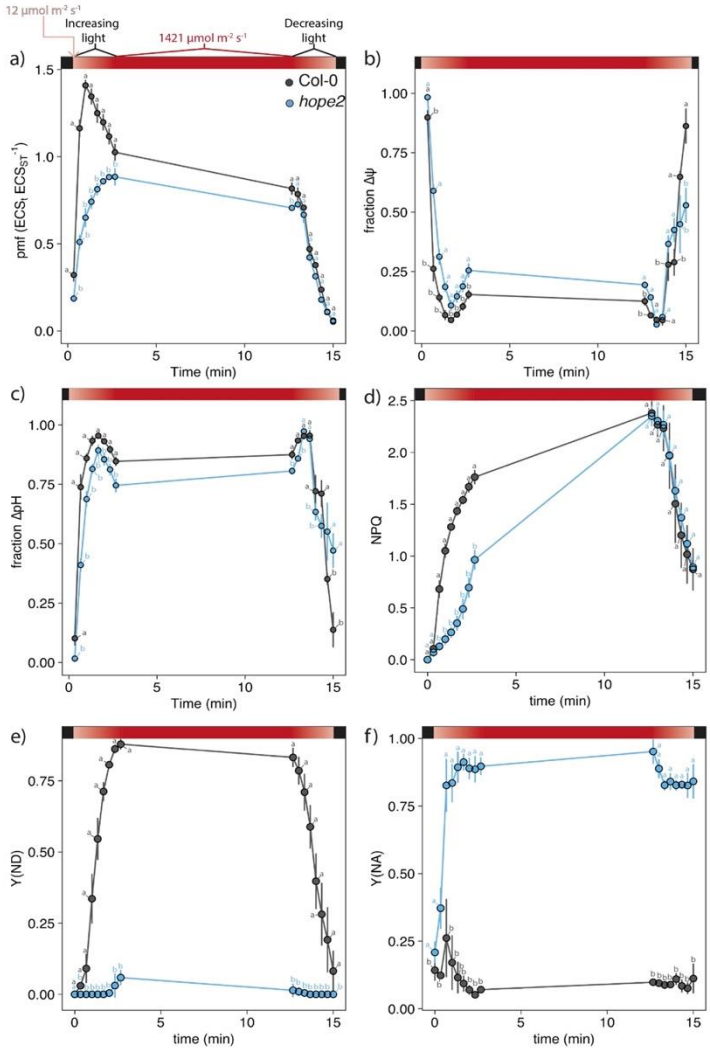

623

624 **Figure 5**: Response of Col-0 and *hope2* to rapidly increasing and decreasing light intensities. a) Proton
625 motive force. b) Fraction of Δψ contribution. c) Fraction of ΔpH contribution. d) Nonphotochemical
626 fluorescence quenching (NPQ). e) Donor-side limitation of PSI (Y(ND)). f) Acceptor-side limitation of

627 PSI (Y(NA)). Rapid changes from low (12 µmol m^{-2} s^{-1}) to high (1421 µmol m^{-2} s^{-1}) light are indicated
628 at the top of panel a by a red color gradient. Light levels were increased every 20 sec, kept at high light
629 for 10 min and decreased every 20 sec. Data points represent the average of 3 biological replicates ±
630 SD. Colors represent genotypes analyzed: Col-0 (black), *hope2* (blue). Different letters indicate
631 statistical significance between genotypes at each light intensity, calculated from a Tukey HSD test,
632 alpha = 0.05.

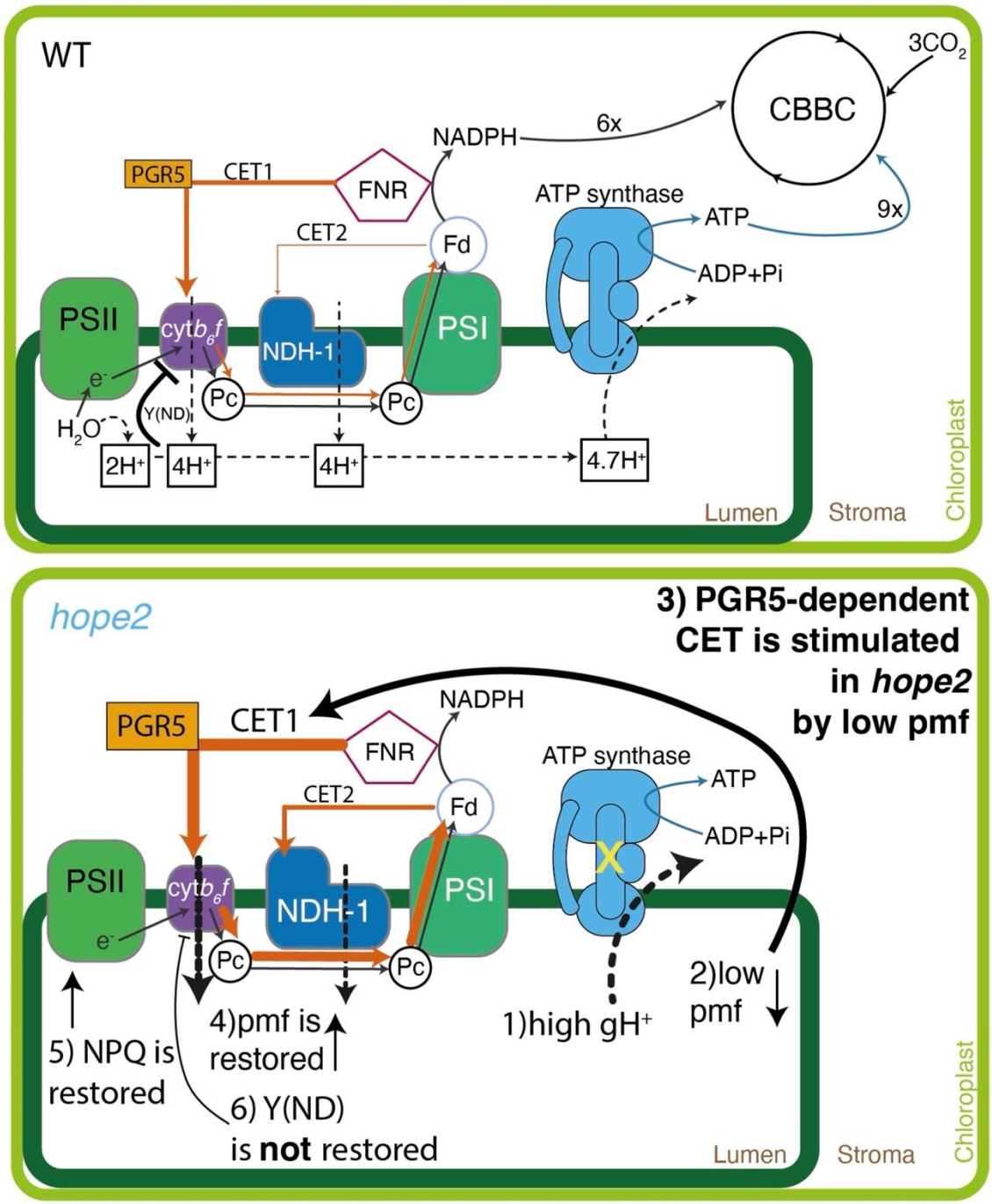

633

634 **Figure 6**: Proposed model of PGR5-dependent supercharged CET in *hope2*. In WT, CET is dominated
635 by PGR5 to produce extra pmf and ATP. CET2 via NDH is more important at low light. Regulation of

636 ATP synthase in *hope2* is disturbed, resulting in high gH^+ and low pmf. In response, PGR5 levels are
637 increased, and to a lesser extent, NDH levels, too. This increases CET1 and restores pmf and NPQ.
638 However, Y(ND) is not restored, suggesting that regulation of ATP synthase is crucial for PSI
639 photoprotection. Abbreviations: PSII, Photosystem II; cytb_6f, cytochrome b_6f complex; NDH-1,
640 NAD(P)H:plastoquinone dehydrogenase complex 1; PSI, Photosystem I; FNR,
641 ferredoxin:NADP(H) oxidoreductase; CBBC, Calvin-Benson-Bassham Cycle; Y(ND), donor-side
642 regulation.

643

644

645 **References**

646 **Alric J, Johnson X** (2017) Alternative electron transport pathways in photosynthesis: a confluence of
647 regulation. Curr Opin Plant Biol **37**: 78–86
648 **Armbruster U, Galvis VC, Kunz H-H, Strand DD** (2017) The regulation of the chloroplast proton
649 motive force plays a key role for photosynthesis in fluctuating light. Curr Opin Plant Biol **37**: 56–62
650 **Avenson TJ, Cruz JA, Kanazawa A, Kramer DM** (2005) Regulating the proton budget of higher
651 plant photosynthesis. P Natl Acad Sci Usa **102**: 9709–9713
652 **Baker NR, Harbinson J, Kramer DM** (2007) Determining the limitations and regulation of
653 photosynthetic energy transduction in leaves. Plant Cell Environ **30**: 1107–1125
654 **Busch FA** (2018) Photosynthetic Gas Exchange in Land Plants at the Leaf Level. Photosynthesis
655 Methods in Molecular Biology **1770**: 25–44
656 **Carrillo LR, Froehlich JE, Cruz JA, Savage LJ, Kramer DM** (2016) Multi-level regulation of the
657 chloroplast ATP synthase: the chloroplast NADPH thioredoxin reductase C (NTRC) is required for
658 redox modulation specifically under low irradiance. Plant J **87**: 654–663
659 **Clark RD, Hawkesford MJ, Coughlan SJ, Bennett J, Hind G** (1984) Association of ferredoxin-
660 NADP+ oxidoreductase with the chloroplast cytochrome b-f complex. Febs Lett **174**: 137–142
661 **Cox J, Mann M** (2008) MaxQuant enables high peptide identification rates, individualized p.p.b.-
662 range mass accuracies and proteome-wide protein quantification. Nat Biotechnol **26**: 1367–1372
663 **DalCorso G, Pesaresi P, Masiero S, Aseeva E, Schünemann D, Finazzi G, Joliot P, Barbato R,**
664 **Leister D** (2008) A Complex Containing PGRL1 and PGR5 Is Involved in the Switch between Linear
665 and Cyclic Electron Flow in Arabidopsis. Cell **132**: 273–285
666 **Davis GA, Kanazawa A, Schöttler MA, Kohzuma K, Froehlich JE, Rutherford AW, Satoh-Cruz**
667 **M, Minhas D, Tietz S, Dhingra A, et al** (2016) Limitations to photosynthesis by proton motive
668 force-induced photosystem II photodamage. Elife **5**: e16921
669 **Dobrescu A, Scorza LCT, Tsaftaris SA, McCormick AJ** (2017) A "Do-It-Yourself" phenotyping
670 system: measuring growth and morphology throughout the diel cycle in rosette shaped plants. Plant

671 Methods **13**: 95
672 **Duursma RA** (2015) Plantecophys - An R Package for Analysing and Modelling Leaf Gas Exchange
673 Data. Plos One **10**: e0143346
674 **Farquhar GD, Caemmerer S von, Berry JA** (1980) A biochemical model of photosynthetic CO2
675 assimilation in leaves of C3 species. Planta **149**: 78–90
676 **Flannery SE, Hepworth C, Wood WHJ, Pastorelli F, Hunter CN, Dickman MJ, Jackson PJ,**
677 **Johnson MP** (2021) Developmental acclimation of the thylakoid proteome to light intensity in
678 Arabidopsis. Plant J **105**: 223–244
679 **Hahn A, Vonck J, Mills DJ, Meier T, Kühlbrandt W** (2018) Structure, mechanism, and regulation
680 of the chloroplast ATP synthase. Science. doi: 10.1126/science.aat4318
681 **Hald S, Nandha B, Gallois P, Johnson GN** (2008) Feedback regulation of photosynthetic electron
682 transport by NADP(H) redox poise. Biochimica Et Biophysica Acta Bba - Bioenergetics **1777**: 433–
683 440
684 **Hepworth C, Wood WHJ, Emrich-Mills TZ, Proctor MS, Casson S, Johnson MP** (2021)
685 Dynamic thylakoid stacking and state transitions work synergistically to avoid acceptor-side
686 limitation of photosystem I. Nature Plants. doi: 10.1038/s41477-020-00828-3
687 **Hertle AP, Blunder T, Wunder T, Pesaresi P, Pribil M, Armbruster U, Leister D** (2013) PGRL1
688 Is the Elusive Ferredoxin-Plastoquinone Reductase in Photosynthetic Cyclic Electron Flow. Mol Cell
689 **49**: 511–523
690 **Hind G, Nakatani HY, Izawa S** (1974) Light-Dependent Redistribution of Ions in Suspensions of
691 Chloroplast Thylakoid Membranes. Proc National Acad Sci **71**: 1484–1488
692 **Hisabori T, Ueoka-Nakanishi H, Konno H, Koyama F** (2003) Molecular evolution of the
693 modulator of chloroplast ATP synthase: origin of the conformational change dependent regulation.
694 Febs Lett **545**: 71–75
695 **Horton P, Ruban AV, Rees D, Pascal AA, Noctor G, Young AJ** (1991) Control of the light-
696 harvesting function of chloroplast membranes by aggregation of the LHCII chlorophyll—protein
697 complex. Febs Lett **292**: 1–4
698 **Jahns P, Graf M, Munekage Y, Shikanai T** (2002) Single point mutation in the Rieske iron–sulfur
699 subunit of cytochrome b 6/f leads to an altered pH dependence of plastoquinol oxidation in
700 Arabidopsis. Febs Lett **519**: 99–102
701 **Johnson GN** (2011) Physiology of PSI cyclic electron transport in higher plants. Biochimica Et
702 Biophysica Acta Bba - Bioenergetics **1807**: 384–389
703 **Johnson GN** (2003) Thiol Regulation of the Thylakoid Electron Transport ChainA Missing Link in
704 the Regulation of Photosynthesis? Biochemistry-us **42**: 3040–3044
705 **Joliot P, Béal D, Joliot A** (2004) Cyclic electron flow under saturating excitation of dark-adapted
706 Arabidopsis leaves. Biochimica Et Biophysica Acta Bba - Bioenergetics **1656**: 166–176
707 **Joliot P, Johnson GN** (2011) Regulation of cyclic and linear electron flow in higher plants. Proc

708 National Acad Sci **108**: 13317–13322
709 **Joliot P, Joliot A** (2002) Cyclic electron transfer in plant leaf. Proc National Acad Sci **99**: 10209–
710 10214
711 **Junesch U, Gräber P** (1987) Influence of the redox state and the activation of the chloroplast ATP
712 synthase on proton-transport-coupled ATP synthesis/hydrolysis. Biochimica et Biophysica Acta
713 (BBA) - Bioenergetics **893**: 275–288
714 **Kanazawa A, Kramer DM** (2002) In vivo modulation of nonphotochemical exciton quenching
715 (NPQ) by regulation of the chloroplast ATP synthase. Proc National Acad Sci 99: 12789–12794
716 **Klughammer C, Schreiber U** (2016) Deconvolution of ferredoxin, plastocyanin, and P700
717 transmittance changes in intact leaves with a new type of kinetic LED array spectrophotometer.
718 Photosynthesis Research. doi: 10.1007/s11120-016-0219-0
719 **Klughammer C, Siebke K, Schreiber U** (2013) Continuous ECS-indicated recording of the proton-
720 motive charge flux in leaves. Photosynthesis Research. doi: 10.1007/s11120-013-9884-4
721 **Kohzuma K, Bosco CD, Kanazawa A, Dhingra A, Nitschke W, Meurer J, Kramer DM** (2012)
722 Thioredoxin-insensitive plastid ATP synthase that performs moonlighting functions. Proc National
723 Acad Sci **109**: 3293–3298
724 **Kohzuma K, Bosco CD, Meurer J, Kramer DM** (2013) Light- and Metabolism-related Regulation
725 of the Chloroplast ATP Synthase Has Distinct Mechanisms and Functions*. J Biol Chem **288**: 13156–
726 13163
727 **Konno H, Nakane T, Yoshida M, Ueoka-Nakanishi H, Hara S, Hisabori T** (2012) Thiol
728 Modulation of the Chloroplast ATP Synthase is Dependent on the Energization of Thylakoid
729 Membranes. Plant Cell Physiol **53**: 626–634
730 **Kramer DM, Avenson TJ, Edwards GE** (2004) Dynamic flexibility in the light reactions of
731 photosynthesis governed by both electron and proton transfer reactions. Trends Plant Sci **9**: 349–357
732 **Kramer DM, Evans JR** (2010) The Importance of Energy Balance in Improving Photosynthetic
733 Productivity . Plant Physiol **155**: 70–78
734 **Kramer M, Rodriguez-Heredia M, Saccon F, Mosebach L, Twachtmann M, Krieger-Liszkay A,**
735 **Duffy C, Knell RJ, Finazzi G, Hanke GT** (2021) Regulation of photosynthetic electron flow on dark
736 to light transition by ferredoxin:NADP(H) oxidoreductase interactions. Elife **10**: e56088
737 **Li Y, Ma X, Weber J** (2019) Interaction between γC87 and γR242 residues participates in energy
738 coupling between catalysis and proton translocation in Escherichia coli ATP synthase. Biochimica Et
739 Biophysica Acta Bba - Bioenergetics **1860**: 679–687
740 **Li Z, Wakao S, Fischer BB, Niyogi KK** (2009) Sensing and Responding to Excess Light. Annu Rev
741 Plant Biol **60**: 239–260
742 **Livingston AK, Cruz JA, Kohzuma K, Dhingra A, Kramer DM** (2010a) An Arabidopsis Mutant
743 with High Cyclic Electron Flow around Photosystem I (hcef) Involving the NADPH Dehydrogenase
744 Complex. Plant Cell Online **22**: 221–233

745 **Livingston AK, Kanazawa A, Cruz JA, Kramer DM** (2010b) Regulation of cyclic electron flow in
746 C3 plants: differential effects of limiting photosynthesis at ribulose-1,5-bisphosphate
747 carboxylase/oxygenase and glyceraldehyde-3-phosphate dehydrogenase. Plant Cell Environ **33**: 1779–
748 1788
749 **Malone LA, Proctor MS, Hitchcock A, Hunter CN, Johnson MP** (2021) Cytochrome b 6 f –
750 Orchestrator of photosynthetic electron transfer. Biochimica Et Biophysica Acta Bba - Bioenergetics
751 **1862**: 148380
752 **Mills JD, Mitchell P** (1982) Modulation of coupling factor ATPase activity in intact chloroplasts.
753 Reversal of thiol modulation in the dark. Biochimica Et Biophysica Acta Bba - Bioenergetics **679**:
754 75–83
755 **Miyake C** (2010) Alternative Electron Flows (Water–Water Cycle and Cyclic Electron Flow Around
756 PSI) in Photosynthesis: Molecular Mechanisms and Physiological Functions. Plant Cell Physiol **51**:
757 1951–1963
758 **Munekage Y, Hashimoto M, Miyake C, Tomizawa K-I, Endo T, Tasaka M, Shikanai T** (2004)
759 Cyclic electron flow around photosystem I is essential for photosynthesis. Nature **429**: 579–582
760 **Munekage Y, Hojo M, Meurer J, Endo T, Tasaka M, Shikanai T** (2002) PGR5 Is Involved in
761 Cyclic Electron Flow around Photosystem I and Is Essential for Photoprotection in Arabidopsis. Cell
762 **110**: 361–371
763 **Nikkanen L, Diaz MG, Toivola J, Tiwari A, Rintamäki E** (2019) Multilevel regulation of non-
764 photochemical quenching and state transitions by chloroplast NADPH-dependent thioredoxin
765 reductase. Physiol Plantarum **166**: 211–225
766 **Nikkanen L, Toivola J, Trotta A, Diaz MG, Tikkanen M, Aro E, Rintamäki E** (**2**018) Regulation
767 of cyclic electron flow by chloroplast NADPH-dependent thioredoxin system. Plant Direct 2: e00093
768 **Nishikawa Y, Yamamoto H, Okegawa Y, Wada S, Sato N, Taira Y, Sugimoto K, Makino A,**
769 **Shikanai T** (2012) PGR5-Dependent Cyclic Electron Transport Around PSI Contributes to the Redox
770 Homeostasis in Chloroplasts Rather Than CO2 Fixation and Biomass Production in Rice. Plant Cell
771 Physiol **53**: 2117–2126
772 **Nishio JN, Whitmarsh J** (1993) Dissipation of the Proton Electrochemical Potential in Intact
773 Chloroplasts (II. The pH Gradient Monitored by Cytochrome f Reduction Kinetics). Plant Physiol
774 **101**: 89–96
775 **Ojeda V, Pérez-Ruiz JM, Cejudo FJ** (2018) 2-Cys Peroxiredoxins Participate in the Oxidation of
776 Chloroplast Enzymes in the Dark. Mol Plant **11**: 1377–1388
777 **Okegawa Y, Long TA, Iwano M, Takayama S, Kobayashi Y, Covert SF, Shikanai T** (2007) A
778 Balanced PGR5 Level is Required for Chloroplast Development and Optimum Operation of Cyclic
779 Electron Transport Around Photosystem I. Plant Cell Physiol **48**: 1462–1471
780 **Okegawa Y, Tsuyama M, Kobayashi Y, Shikanai T** (2005) The pgr1 Mutation in the Rieske
781 Subunit of the Cytochrome b 6 f Complex Does Not Affect PGR5-dependent Cyclic Electron

782 Transport around Photosystem I*. J Biol Chem **280**: 28332–28336
783 **Ort DR, Oxborough K** (1992) In Situ Regulation of Chloroplast Coupling Factor Activity. Annu
784 Rev Plant Phys **43**: 269–291
785 **Penzler J-F, Marino G, Reiter B, Kleine T, Naranjo B, Leister D** (2022) Commonalities and
786 specialties in photosynthetic functions of PROTON GRADIENT REGULATION5 variants in
787 Arabidopsis. Plant Physiol. doi: 10.1093/plphys/kiac362
788 **Rantala S, Lempiäinen T, Gerotto C, Tiwari A, Aro E-M, Tikkanen M** (2020) PGR5 and NDH-1
789 systems do not function as protective electron acceptors but mitigate the consequences of PSI
790 inhibition. Biochimica Et Biophysica Acta Bba - Bioenergetics **1861**: 148154
791 **Rees D, Young A, Noctor G, Britton G, Horton P** (1989) Enhancement of the ΔpH-dependent
792 dissipation of excitation energy in spinach chloroplasts by light-activation: correlation with the
793 synthesis of zeaxanthin. Febs Lett **256**: 85–90
794 **Rott M, Martins NF, Thiele W, Lein W, Bock R, Kramer DM, Schöttler MA** (2011) ATP
795 Synthase Repression in Tobacco Restricts Photosynthetic Electron Transport, CO2 Assimilation, and
796 Plant Growth by Overacidification of the Thylakoid Lumen. Plant Cell **23**: 304–321
797 **Ruban AV, Johnson MP, Duffy CDP** (2012) The photoprotective molecular switch in the
798 photosystem II antenna. Biochimica et biophysica acta **1817**: 167–181
799 **Rühle T, Dann M, Reiter B, Schünemann D, Naranjo B, Penzler J-F, Kleine T, Leister D** (2021)
800 PGRL2 triggers degradation of PGR5 in the absence of PGRL1. Nat Commun **12**: 3941
801 **Rumeau D, Bécuwe-Linka N, Beyly A, Louwagie M, Garin J, Peltier G** (2005) New Subunits
802 NDH-M, -N, and -O, Encoded by Nuclear Genes, Are Essential for Plastid Ndh Complex Functioning
803 in Higher Plants. Plant Cell **17**: 219–232
804 **Schreiber U, Klughammer C** (2016) Analysis of Photosystem I Donor and Acceptor Sides with a
805 New Type of Online-Deconvoluting Kinetic LED-Array Spectrophotometer. Plant and Cell
806 Physiology. doi: 10.1093/pcp/pcw044
807 **Schwanhäusser B, Busse D, Li N, Dittmar G, Schuchhardt J, Wolf J, Chen W, Selbach M** (2011)
808 Global quantification of mammalian gene expression control. Nature **473**: 337–342
809 **Sekiguchi T, Yoshida K, Okegawa Y, Motohashi K, Wakabayashi K, Hisabori T** (2020)
810 Chloroplast ATP synthase is reduced by both f-type and m-type thioredoxins. Biochimica Et
811 Biophysica Acta Bba - Bioenergetics **1861**: 148261
812 **Shahak Y, Crowther D, Hind G** (1981) The involvement of ferredoxin-NADP+ reductase in cyclic
813 electron transport in chloroplasts. Biochimica Et Biophysica Acta Bba - Bioenergetics **636**: 234–243
814 **Shen L, Tang K, Wang W, Wang C, Wu H, Mao Z, An S, Chang S, Kuang T, Shen J-R, et al**
815 (2022) Architecture of the chloroplast PSI–NDH supercomplex in Hordeum vulgare. Nature **601**:
816 649–654
817 **Strand DD, Fisher N, Davis GA, Kramer DM** (2016) Redox regulation of the antimycin A sensitive
818 pathway of cyclic electron flow around photosystem I in higher plant thylakoids. Biochimica Et

819 Biophysica Acta Bba - Bioenergetics **1857**: 1–6
820 **Strand DD, Livingston AK, Satoh-Cruz M, Froehlich JE, Maurino VG, Kramer DM** (2015)
821 Activation of cyclic electron flow by hydrogen peroxide in vivo. Proc National Acad Sci **112**: 5539–
822 5544
823 **Strand DD, Livingston AK, Satoh-Cruz M, Koepke T, Enlow HM, Fisher N, Froehlich JE, Cruz**
824 **JA, Minhas D, Hixson KK, et al** (2017) Defects in the Expression of Chloroplast Proteins Leads to
825 H2O2 Accumulation and Activation of Cyclic Electron Flow around Photosystem I. Front Plant Sci 7:
826 2073
827 **Su X, Cao D, Pan X, Shi L, Liu Z, Dall'Osto L, Bassi R, Zhang X, Li M** (2022) Supramolecular
828 assembly of chloroplast NADH dehydrogenase-like complex with photosystem I from Arabidopsis
829 thaliana. Mol Plant **15**: 454–467
830 **Suorsa M, Grieco M, Järvi S, Gollan PJ, Kangasjärvi S, Tikkanen M, Aro E-M** (2013) PGR5
831 ensures photosynthetic control to safeguard photosystem I under fluctuating light conditions. Plant
832 Signal Behav **8**: e22741
833 **Suorsa M, Järvi S, Grieco M, Nurmi M, Pietrzykowska M, Rantala M, Kangasjärvi S,**
834 **Paakkarinen V, Tikkanen M, Jansson S, et al** (2012) PROTON GRADIENT REGULATION5 Is
835 Essential for Proper Acclimation of Arabidopsis Photosystem I to Naturally and Artificially
836 Fluctuating Light Conditions. Plant Cell Online **24**: 2934–2948
837 **Takagi D, Amako K, Hashiguchi M, Fukaki H, Ishizaki K, Goh T, Fukao Y, Sano R, Kurata T,**
838 **Demura T, et al** (2017) Chloroplastic ATP synthase builds up a proton motive force preventing
839 production of reactive oxygen species in photosystem I. Plant J **91**: 306–324
840 **Takagi D, Miyake C** (2018) PROTON GRADIENT REGULATION 5 supports linear electron flow
841 to oxidize photosystem I. Physiol Plantarum **164**: 337–348
842 **Takizawa K, Cruz JA, Kanazawa A, Kramer DM** (2007) The thylakoid proton motive force in
843 vivo. Quantitative, non-invasive probes, energetics, and regulatory consequences of light-induced
844 pmf. Biochimica Et Biophysica Acta Bba - Bioenergetics **1767**: 1233–1244
845 **Takizawa K, Kanazawa A, Kramer DM** (2008) Depletion of stromal Pi induces high 'energy-
846 dependent' antenna exciton quenching (qE) by decreasing proton conductivity at CFO-CF1 ATP
847 synthase. Plant Cell Environ **31**: 235–243
848 **Velthuys BR** (1978) A third site of proton translocation in green plant photosynthetic electron
849 transport. Proc National Acad Sci **75**: 6031–6034
850 **Wada S, Amako K, Miyake C** (2021) Identification of a Novel Mutation Exacerbated the PSI
851 Photoinhibition in pgr5/pgrl1 Mutants; Caution for Overestimation of the Phenotypes in Arabidopsis
852 pgr5-1 Mutant. Cells **10**: 2884
853 **Wang C, Takahashi H, Shikanai T** (2018) PROTON GRADIENT REGULATION 5 contributes to
854 ferredoxin-dependent cyclic phosphorylation in ruptured chloroplasts. Biochimica Et Biophysica Acta
855 Bba - Bioenergetics **1859**: 1173–1179

Wang C, Yamamoto H, Shikanai T (2015) Role of cyclic electron transport around photosystem I in regulating proton motive force. Biochimica Et Biophysica Acta Bba - Bioenergetics **1847**: 931–938

Wilson S, Johnson MP, Ruban AV (2021) Proton motive force in plant photosynthesis dominated by ΔpH in both low and high light. Plant Physiol **187**: 263–275

Yamamoto H, Shikanai T (2020) Does the Arabidopsis proton gradient regulation 5 mutant leak protons from the thylakoid membrane? Plant Physiol 184: pp.00850.2020

Yamamoto H, Takahashi S, Badger MR, Shikanai T (**2**016) Artificial remodelling of alternative electron flow by flavodiiron proteins in Arabidopsis. Nat Plants 2: 16012

Yamori W, Makino A, Shikanai T (201**6**) A physiological role of cyclic electron transport around photosystem I in sustaining photosynthesis under fluctuating light in rice. Sci Rep-uk 6: 20147

Yamori W, Sakata N, Suzuki Y, Shikanai T, Makino A (2011) Cyclic electron flow around photosystem I via chloroplast NAD(P)H dehydrogenase (NDH) complex performs a significant physiological role during photosynthesis and plant growth at low temperature in rice. Plant J **68**: 966–976

Yamori W, Shikanai T (2015) Physiological Functions of Cyclic Electron Transport Around Photosystem I in Sustaining Photosynthesis and Plant Growth. Annu Rev Plant Biol **67**: 1–26

Yamori W, Shikanai T, Makino A (201**5**) Photosystem I cyclic electron flow via chloroplast NADH dehydrogenase-like complex performs a physiological role for photosynthesis at low light. Sci Rep-uk 5: 13908

Yu F, Haynes SE, Nesvizhskii AI (**20**21) IonQuant Enables Accurate and Sensitive Label-Free Quantification With FDR-Controlled Match-Between-Runs. Mol Cell Proteomics 20: 100077

Zhang H, Whitelegge JP, Cramer WA (2001) Ferredoxin:NADP+ Oxidoreductase Is a Subunit of the Chloroplast Cytochrome b6fComplex*. J Biol Chem **276**: 38159–38165

Zhou Q, Wang C, Yamamoto H, Shikanai T (2022) PTOX-dependent safety valve does not oxidize P700 during photosynthetic induction in the Arabidopsis pgr5 mutant. Plant Physiol **188**: 1264–1276